
Article:
Deeth, RJ, Halcrow, MA orcid.org/0000-0001-7491-9034, Kershaw Cook, LJ et al. (1 more author) (2018) Ab Initio Ligand Field Molecular Mechanics and the Nature of Metal-Ligand π-Bonding in Fe(II) 2,6-di(pyrazol-1-yl)pyridine Spin Crossover Complexes. Chemistry - A European Journal, 24 (20). pp. 5204-5212. ISSN 0947-6539

https://doi.org/10.1002/chem.201704558

Revised manuscript: chem.201704558

Ab Initio Ligand Field Molecular Mechanics and the Nature of Metal-Ligand π-Bonding in Fe(II) 2,6-di(pyrazol-1-yl)pyridine Spin Crossover Complexes

Robert J. Deeth[1,2]*, Malcolm A. Halcrow[3], Laurence J. Kershaw Cook[2] and Paul R. Raithby[2]

[1] Department of Chemistry, University of Warwick, Coventry CV4 7AL, UK

[2] Department of Chemistry, University of Bath, Claverton Down, Bath BA2 7AY

[3] School of Chemistry, University of Leeds, Leeds, LS2 9JT, UK

E-mail: r.j.deeth@warwick.ac.uk

Abstract

A ligand field molecular mechanics (LFMM) force field has been constructed for the spin states of $[Fe(bpp)_2]^{2+}$ (bpp = 2,6-di(pyrazol-1-yl)pyridine) and related complexes. A new charge scheme is employed which interpolates between partial charges for neutral bpp and protonated $[H_3bpp]^{3+}$ to achieve a target metal charge. The LFMM angular overlap model (AOM) parameters are fitted to fully ab initio d orbital energies. However, several AOM parameters sets are possible. The ambiguity is resolved by calculating the Jahn-Teller distortion mode for high spin which indicates that in $[Fe(bpp)_2]^{2+}$pyridine is a π acceptor and pyrazole a weak π donor. The alternative fit, assumed previously, where both ligands act as π donors leads to an inconsistent distortion. LFMM optimisations in the presence of $[BF_4]^-$ or $[PF_6]^-$ anions are in good agreement with experiment and the model also correctly predicts the spin state energetics for 3-pyrazolyl substituents where the interactions are mainly steric. However, for 4-pyridyl or 4-pyrazolyl substituents, LFMM only treats the electrostatic contribution which, for the pyridyl substituents, generates a fair correlation with the spin crossover transition temperatures, $T_{1/2}$, but in the reverse sense to the dominant electronic effect. Thus, LFMM generates its smallest spin state energy difference for the substituent with the highest $T_{1/2}$. One parameter set for all substituted bpp ligands is insufficient and further LFMM development will be required.

Introduction

The spin crossover (SCO) phenomenon is a fascinating feature of coordination chemistry.[1] The ability to switch the spin state at the metal centre in response to an external stimulus promises many potential applications in electronic devices and sensors.[2] SCO arises from a delicate energetic balance between two electronic states of metal centres which have the right combination of d configuration, ligand donor set and coordination geometry.[1b, 3] Historically, the first SCO systems were found serendipitously.[4] Since then, concerted efforts have been made to design new SCO systems rationally.[5]

SCO is conceptually relatively simple with the essential issues were detailed by van Vleck in 1935.[6] For the archetypal octahedral d^6 Fe(II) case, there are two relevant spin states, high spin (HS) $^5T_{2g}$ and low spin (LS) $^1A_{1g}$. The LS state is preferentially stabilised by the one-electron crystal field stabilisation energy (CFSE) and is $2\Delta_{oct}$ lower that the HS state. The HS state is preferentially stabilised by the (two-electron) exchange energy arising from the greater number of unique pairs of parallel spins (10) compared to only 6 pairs for LS. The HS state also has higher entropy. Thus, if at low temperature the LS state is a few kcal mol^{-1} below HS, then, as the temperature is raised, the HS state is increasingly stabilised and at some point becomes the new ground state. This is thermal SCO[1c] with the midpoint temperature at which there are equal mole fractions of HS and LS denoted $T_{1/2}$.

Since the HS Fe-L bond lengths are significantly longer (~0.2 Å) than their LS counterparts, applying pressure can also effect a spin transition.[7] Perhaps more significantly, some systems in their low-temperature, LS form can be excited by light into the HS state. If the temperature is kept low enough, the HS state may become 'trapped' leading to light-induced excited spin state trapping (LIESST).[8] LIESST provides a mechanism for optical spin state switching.

Irrespective of how the SCO transition occurs, solid state effects are of crucial importance.[1c, 9] In thermal SCO, the change in molecular volume can alter the cooperativity between metal-containing units generating hysteresis – i.e. the temperature at which the spin transition occurs is different for heating (↑) and cooling (↓) cycles and $T_{1/2}(\uparrow) \neq T_{1/2}(\downarrow)$. This hysteretic 'memory effect' leads to bistability which is highly desirable for practical devices.

As with any molecular discovery process, computational chemistry has a potentially important role to play in SCO. Given the inherent complexities of the electronic structures of open-shell TM species, most of the modelling effort has focused on quantum chemical (QC)

methods.[10] Many QC protocols provide good qualitative results but the extreme sensitivity of SCO to electronic exchange means that both wavefunction methods and density functional theory struggle with *absolute* spin state energy differences and the search for a 'universal' theoretical approach is ongoing.[11] SCO is even more challenging in that even if the perfect method for computing the spin state energies of potential SCO complexes were available, the critical role played by environmental effects such as crystal packing, incorporated solvents, etc. essentially demands that we be able to predict the full crystal structure from first principles; a task which is beyond present capabilities. The best that can be currently hoped for is to identify metal complexes which, in isolation but *not* in vacuo,[12] have the right spin state energetics to *potentially* support SCO and trust that this behaviour will survive in the crystalline state.[13]

This 'uncertainty' can be used to advantage since, as mentioned above, many computational methods give the correct trends and so can be usefully employed for predicting qualitative changes in spin state energetics. Hence, given a system with a particular ground state spin, we can use computational chemistry to design modifications which should direct the spin state energetics to change in the desired direction. In this spirit, therefore, we have developed an empirical force field approach – ligand field molecular mechanics (LFMM)[14] – which explicitly considers the one-electron CFSE and the two-electron exchange terms to facilitate the rapid screening of large numbers of TM complexes for potential SCO behaviour. As a proof-of-concept, an LFMM force field (FF) for Fe(II)-amine complexes was designed to reproduce the experimentally-observed trend in spin states for a small set of complexes.[15] This FF was then exploited in a fragment-based virtual high-throughput screen to identify hitherto unknown SCO species.[16] As will be reported elsewhere,[17] the complex with the highest theoretical 'fitness', $[Fe(tame)_2]^{2+}$, (tame = 1,1,1-tris(aminomethyl)ethane)) displays SCO behaviour experimentally.

Our prior work has focussed almost exclusively on simple, σ-donor-only amines connected via saturated alkane backbones. However, the majority of actual Fe(II) SCO systems employ unsaturated N donors, often incorporated into delocalised ring systems where substituents well removed from the metal centre exert significant electronic effects on the metal-ligand bonding. These more complicated systems require more parameters and we address this issue in the current work.

The utility of any force field method is determined by the accuracy and transferability of its parameters.[18] A minimal, conventional, valence FF comprises a number of terms describing

the strain energy associated with bond stretching, angle bending, torsional twisting, and non-bonding interactions. More sophisticated FFs may also include other terms such as improper dihedrals, out-of-plane terms, stretch-bend terms and so on. Each term in turn requires a number of empirical parameters and, depending on the richness of the supported atom types, may result in a FF of many thousands of parameters.

Attempts to generate more generic FFs which use atom-centred quantities to generate suitable parameters for molecular systems have been made, with the universal force field[19] probably being the most popular, but these are generally of lower accuracy than bespoke valence FFs. This is particularly the case for transition metal (TM) systems which are especially difficult for conventional valence FFs.[14b, 20]

The d electrons exert significant structural and energetic influence in coordination complexes[14a] and any computational scheme needs to account for them explicitly or implicitly. Density functional theory (DFT) is the most used form of quantum chemistry and includes electronic effects implicitly. However, in common with all QC methods, DFT is relatively slow. In contrast, our approach has been to extend MM by incorporating an explicit, generalised ligand field (LF) treatment of d electron effects directly into the FF framework. The LF component is based on the angular overlap model (AOM).[21] The resulting ligand field molecular mechanics (LFMM) approach has been successfully applied to a number of TM systems[20, 22] but the issue of parameterisation is even more problematic since, in addition to the 'normal' FF terms, each metal-ligand interaction attracts up to five additional parameters to describe the d-electron contribution.[23] In this work, we describe a procedure based on advanced wavefunction methodology[24] which allows us to derive AOM parameter sets without recourse to any experimental data and explicitly test their description of the nature of the metal-ligand bonding interactions.

Computational details

All quantum chemical calculations employed the ORCA program suite, either version 3.0.3[25] for general DFT calculations or a pre version 4 release for the ab initio ligand field theory (AILFT)[24a, 26] (*vide infra*) calculations. The general DFT protocol was the same as in our previous study[5b] and involved geometry optimisation using the BP86 functional[27] with the resolution of identity approximation and def2-SVP basis sets.[28] Environmental effects were treated via the conductor-like screening model[29] with acetone as solvent.

The AILFT calculations[24a, 26] for a d^n system employ a complete active space SCF (CASSCF) calculation on a *n* electron, five orbitals (*n*,5) active space restricted to the five 'mainly-d' molecular orbitals (MOs) followed by an n-electron valence state 2nd order perturbation theory (NEVPT2) treatment of dynamical correlation. A similar approach, at least in spirit but using DFT, was proposed earlier by Daul[30] based on Ziegler, Rauk and Baerends' method for computing multiplet states[31] which in turn exploits Slater's analysis that DFT remains valid even for non-integral orbital occupations.[32] Atanasov and Daul further developed and applied Ligand field DFT[33] and recent applications by Gruden-Pavlovic and co-workers have achieved some impressive results.[34]

Returning to AILFT, the populations of the active orbitals are constrained to *n*/5 (for Fe(II), *n* = 6) and thus emulate the "spherical configuration" implicit in ligand field theory.[35] The active space for a d^6 Fe(II) complex thus spans the full set of states with a total degeneracy of 210 comprising five spin quintets (^{5}D), 45 spin triplets (2 x ^{3}P, ^{3}D, 2 x ^{3}F, ^{3}G, ^{3}H) and 50 spin singlets (2 x ^{1}S, 2 x ^{1}D, ^{1}F, 2x ^{1}G, ^{1}I). The CASSCF/NEVPT2 energies (def2-TZVP basis sets) of all these multiplets can then be mapped directly onto the equivalent ligand field description which expresses the multiplet energies in terms of the matrix elements of the ligand field potential, V_{LF}, and the interelectron repulsion parameters, here, Racah B and C. Spin-orbit coupling can also be included but this has not been done here. The LF parameters can then be fitted to the AILFT state energies.

The DFT-optimised structures were used as input coordinates and the relevant MOs were identified for the LS electronic configuration for both HS and LS geometries as those with greater than 70% d character. In the LS case, the notional e_g orbitals were not the LUMO and LUMO+1 and needed to be rotated to conform with ORCA's requirement that the active space orbitals span the HOMO-LUMO region.

Diagonalisation of the resulting V_{LF} matrix generates a set of one-electron d orbital energies which are ideally suited to a subsequent AOM[21] analysis akin to a conventional ligand field analysis[36] except that the AOM parameters are now fitted to theoretical d orbital energies rather than those derived from experimental spectroscopic and/or magnetic measurements. All AOM calculations employed the CAMMAG[37] program version 4.5 within a d^1 (^{2}D) basis. The application of this AILFT/AOM method to the electronic structure of FeS_4 systems has recently been reported.[38]

Ligand field molecular mechanics (LFMM) calculations employed DommiMOE,[39] our extension of the 2015 version of the molecular operating environment (MOE).[40] Electrostatic interactions are treated using the R-field method implemented in MOE with no distance cutoffs.

Results and discussion

Historically, AOM parameters were usually derived by classical ligand field analysis wherein the experimental electronic spectrum and magnetic properties of a complex of known structure were reproduced by fitting to computed data.[41] Ligand field theory is a projection operator scheme.[35] As shown in equation (1), the LF Hamiltonian, H'_{LF}, comprises three terms describing the d-d interelectron repulsion, $U(i, j)$, spin-orbit coupling ($\mathbf{l}_i \bullet \mathbf{s}_i$) and the ligand field potential, V_{LF}.

$$H'_{LF} = \sum_{i<j}^{N} U(i,j) + \sum_{i}^{N} V_{LF}(\mathbf{r}_i) + \zeta \sum_{i}^{N} \mathbf{l}_i \cdot \mathbf{s}_i \qquad (1)$$

These terms operate on a set of states associated with a given d configuration. Since the d symmetry label formally refers to spherical symmetry, the first two terms of equation (1) assume a central field (i.e. spherical) approximation and only V_{LF} contains any information about the true molecular symmetry. Trivially, V_{LF} may be separated into spherical and non-spherical components. The crucial feature, therefore, is that in order for LFT to work, the spherical part of V_{LF} must be much larger than the non-spherical part otherwise the central field approximation used for the other terms in the Hamiltonian would break down.[42] In practice, LFT works best for more-or-less ionic Werner-type complexes where the formal d configuration is well defined.

Given sufficient experimental data, unique AOM parameter values can often be extracted and used to describe the nature of the metal-ligand σ and π bonding interactions.[42] However, this process is also symmetry dependent. While there are 15 unique matrix elements and thus 14 degrees of freedom in V_{LF} - we are only concerned with energy differences - this does not mean that 14 independent AOM parameters can be fitted. For example, in perfect octahedral symmetry the d orbitals split into e_g and t_{2g} sets separated by Δ_{oct}. There is only one degree of freedom but even a simple ligand like chloride has two AOM parameters, e_σ and e_π with Δ_{oct} given by $3e_\sigma$-$4e_\pi$. The problem is inherently underdetermined and unique values for both can never be derived simultaneously irrespective of the amount of experimental data available.

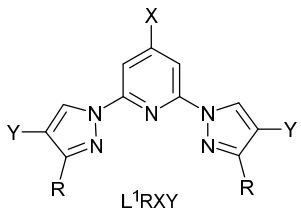

Scheme 1

Iron(II) complexes of 2,6-di(pyrazol-1-yl)pyridine (**L^{1}RXY** or bpp, Scheme 1) present similar problems. For R, X and Y = H, (**1**) the highest symmetry possible is D_{2d} which generates a ligand field with exactly three degrees of freedom. However, the experimental d-d spectra and magnetic susceptibility measurements are unable to resolve this fully. Detailed single crystal measurements might improve this situation but are not available. We turn therefore to theory.

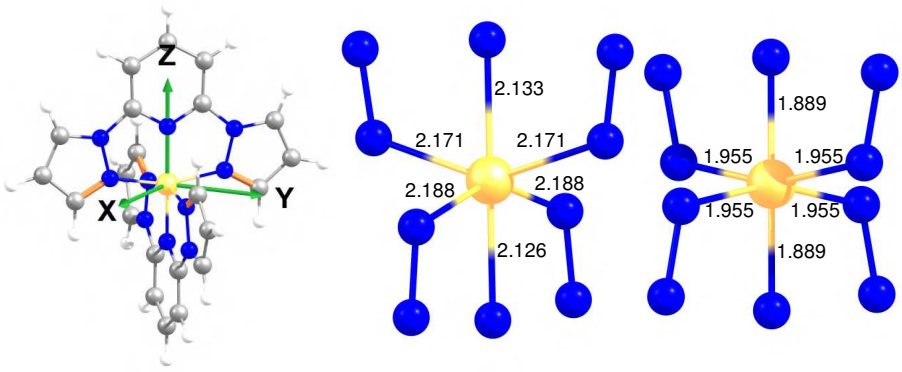

Figure 1 Axis frame definition for $[Fe(bpp)_2]^{2+}$ systems (left). Atoms and bond length data used to set up CAMMAG calculations for HS (centre) and LS (right) systems

HS and LS forms of $[Fe(\mathbf{L^1}HHH)_2]^{2+}$ (**1**) were optimised using the BP86/SVP/COSMO(acetone) protocol employed previously.[5b] The computed structures are in good agreement with experiment although for the HS case, the Jahn-Teller distortions arising from crystal packing and/or intermolecular interactions generate some variation in the reported geometries. Compared to **1[BF$_4$]$_2$** at 300K for HS or 150K for LS,[43] the DFT-optimised Fe-N distances are systematically shorter than experiment but only by 0.01-0.03 Å. The DFT HS form has C_{2v} symmetry with slightly inequivalent chelate coordination, consistent with a Jahn-Teller effect for the parent octahedral $^5T_{2g}$ state, while the orbitally non-degenerate LS form has equivalent ligands and D_{2d} symmetry. Numerical frequencies confirmed that both structures are local minima (see Supporting Information for coordinates and vibrational data, Tables S1 to S4).

The DFT-optimised structures for HS and LS **1** are oriented with the Z axis aligned along the Fe-N(pyridine) direction and X and Y bisecting the equatorial N-Fe-N angles (Figure 1, left).

This allows for easy identification of any d orbitals but means that d_{xy} is the equatorial σ orbital while d_{x2-y2} is aligned with the out-of-plane pyrazolyl π orbitals, although the interaction is reduced from its maximum value since the ~73-80 ° N(py)-Fe-N(pyz) bite angles raise the pyrazolyl N donors out of the XY plane.

The DFT coordinates were used to set up CAMMAG[37] AOM calculations (Figure 1, middle and right and Supporting Information). Only two unique ligand types are considered: pyridine (py) and pyrazole (pyz). Each ligand requires e_σ for the M-L σ bonding, a π-bonding parameter to describe the M-L π interaction perpendicular to the ligand plane, $e_{\pi\perp}$, and a second-order d-s mixing parameter, e_{ds}.[44] Six AOM parameters are required in total.

Systematic variation of the six parameters defines the dependence of the d orbital energy differences on each of the AOM parameters (see Supporting Information, Table S5 and S6). The dependence is analytic for e_σ and $e_{\pi\perp}$ but more complicated for the second-order e_{ds} parameter. Symmetry dictates that the d-s mixing term only affects the d_{z2} orbital[44] since it has the same symmetry as the metal s function. However, the energy shift of d_{z2} depends not only on the magnitudes of e_{ds}(py) and e_{ds}(pyz) but also on their difference. The spreadsheet used to fit the AOM parameters thus employs an approximate equation for the dependence of the d_{z2} energy on the e_{ds} parameter values with the final results checked with explicit CAMMAG calculations.

In LFMM, the AOM parameters depend on the M-L distances. Here, we assume a_6/r^6 or a_5/r^5 variations and the a_i parameters are varied to get a reasonable fit between the ab initio ligand field theory d-orbital energy differences (*vide infra* and see Supporting Information Table S9) and those generated from the AOM. Given the assumptions in the model, it is not possible to get perfect agreement. However, a number of trends emerge some of which can be deduced by considering the d orbital energies for a hypothetical complex where the pyrazole nitrogens lie perfectly in the XY plane. Under these circumstances, the d orbital energies as functions of the AOM parameters are:

$E(d_{xz}/d_{yz}) = e_{\pi\perp}(py)$

$E(d_{x2-y2}) = 4e_{\pi\perp}(pyz)$

$E(d_{xy}) = 3e_\sigma(pyz)$

$E(d_{z2}) = 2e_\sigma(py)+e_\sigma(pyz) - 4\{e_{ds}(py)+e_{ds}(pyz)\} + 8\{e_{ds}(py)-e_{ds}(pyz)\}^{1/2}$

Given the high symmetry, there is a good separation between σ and π bonding effects. Since d_{z2} turns out to be higher than d_{xy}, e_σ(py) is larger than e_σ(pyz). For the (mainly) π functions, AILFT places d_{xz}/d_{yz} lower than d_{x2-y2} (Table 2) which, qualitatively, can be achieved in a number of ways: a) if both ligands are π donors (i.e. $e_\pi > 0$), then $e_{\pi\perp}$(pyz) needs to be greater than ~0.25 $e_{\pi\perp}$(py); both ligands could therefore be moderate to strong π donors as was assumed previously[43b]; b) conversely, if both ligands are π acceptors, the pyridine will have to be a much stronger π acceptor that pyrazole to depress the d_{xz}/d_{yz} orbitals below d_{x2-y2}; c) if pyridine acts as a π acceptor while pyrazole is a π donor, d_{xz}/d_{yz} lower than d_{x2-y2} is guaranteed; d) a π donor pyridine in combination with a π acceptor pyrazole is ruled out completely.

Automatic least-squares fitting gives scenario c) (parameter Set A in Table 1). However, the results are somewhat sensitive to the model, especially the chosen Fe-N bond lengths which are themselves derived from the DFT optimisations. Allowing for, say, a 0.02 Å uncertainty in the bond lengths, which is comparable to the difference between DFT and single crystal X-ray diffraction studies as described above, leads to changes in computed d-orbital energy differences of up to 1000 cm^{-1} for d_{xy} and d_{z2}. It is thus possible to find a scenario a) solution of comparable quality (Set B in Table 1).

A feature of both Set A and Set B is that the AOM results tend to place d_{xy} higher than AILFT for HS but lower than AILFT for LS by several hundred wavenumbers (Table 2). The spectrum of **1** in solution shows a d-d band centred at 10400 cm^{-1} split into two components at 9700 with a shoulder at 11100 cm^{-1}.[43b] However, given that AILFT energy differences often deviate from experimental values by up to a few thousand wavenumbers[24a, 26b, 45] and here predicts the d-d bands to be at ~7400 and ~9000 cm^{-1}, it cannot be stated with any certainty which approach, AILFT or AOM, is 'correct'. Suffice it to say that the fits are satisfactory for a qualitative discussion of the metal-ligand bonding, but are by no means unique.

AOM par	*Set A: HS*	*Set A: LS*	*Set B: HS*	*Set B: LS*
$e_\sigma(py)$	3811	7809	4444	9105
$e_{\pi\perp}(py)$	-841	-1503	684	1244
$e_{ds}(pyz)$	2005	4109	1820	3730
$e_\sigma(pyz)$	3280	6210	3866	7320
$e_{\pi\perp}(pyz)$	196	334	691	1175
$e_{ds}(pyz)$	2880	5453	2981	5644

Table 1 Representative AOM parameter sets which generate d-orbital energy differences shown in Table 2.

Orbital	*E(AILFT): HS*	*Set A: HS ΔE(AOM-AILFT)*	*Set B: HS ΔE(AOM-AILFT)*	*E(AILFT): LS*	*Set A: LS ΔE(AOM-AILFT)*	*Set B: LS ΔE(AOM-AILFT)*
d_{xy}/d_{yz}	***0/193***	0/-58	0/-42	***0/0***	0/0	0/1
d_{x2-y2}	***237***	38	-54	***1698***	140	420
d_{xy}	***7354***	493	146	***18841***	-661	-501
d_{z2}	***8992***	-1	-184	***21311***	36	375

Table 2 AILFT d-orbital energies differences E(AILFT), and the difference between AOM and AILFT energies ΔE(AOM-AILFT) for parameter Sets A and B in Table 1.

The a_i parameters and Fe-N bond lengths upon which the parameters in Table 1 are based can now be used as part of the LFMM treatment.

Partial atomic charges are a critical part of any force field.[18b] In this work, we introduce a new scheme aimed at generating an internally consistent set of charges based on a given force field's treatment of protonation. We use the MMFF[46] scheme as implemented in MOE since it has explicit partial charges for deprotonated and protonated forms of heterocyclic donors such as pyridine and pyrazole. The final partial charges are interpolated between the unprotonated and protonated forms of the ligands in such a way as to generate a target partial charge on the metal. These interpolated partial charges are thus derived directly from the MMFF charges rather than imposed via some other procedure such as Mulliken charges. The protonation-scaled metal-ligand (PMSL) scheme is initially set for six amine donors. When protonated, the MMFF amine H atom carries a charge of 0.45 implying that 0.55 of an electron has been 'donated' from the ligand – that is, 3.3 in total for a FeN_6 moiety. The target charge on the metal was determined from a natural orbital analysis of HS and LS $[Fe(en)_3]^{2+}$ (en = ethylenediamine) to be 1.3. The required charge donation is thus 0.7 which equates to 0.7/3.3 or 21%. Hence, the final ligand charges will be 79% of the neutral-ligand values plus 21% of the fully-protonated version (Figure 2). Of course, the final charges depend on the choice of target metal charge but the latter is a feature of all TM force fields. The PMSL scheme has the advantage that once the decision concerning the metal charge is made, the resulting charge scheme is matched to MMFF electrostatics.

The PMSL scheme should be transferable to other ligands since it responds to variations in proton charge for other N donors. The MMFF partial charge for a pyrazole proton is the same as for an amine (0.45) but that for a pyridine proton is slightly more positive (0.457) which results in the Fe charge in **1** of 1.314 (Figure 2).

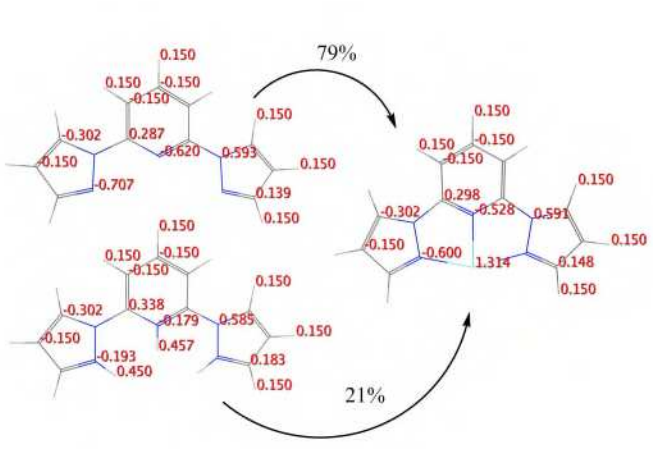

Figure 2 Protonation-scaled metal-ligand charge data for complex **1**. Top left: MMFF charges for unprotonated ligand. Bottom left: MMFF charges for fully protonated ligand. Right: final MMFF interpolated charges which results in an Fe partial charge of 1.314. (Only symmetry unique atoms are labelled to avoid cluttering the figure.)

With the partial charges and AOM parameters set, the remaining LFMM parameters can be optimised. The Morse function α and D parameters are not independent, so the dissociation energy is fixed and only α is varied. The ligand-ligand repulsion term has the form A_{LL}/d^n where d are the distances between donor atoms. As previously,[23] n is set to 6 and the A_{LL} values varied. Finally, the interelectron repulsion energy is treated as a simple penalty function with the same mathematical form as the AOM e parameters. In this work, the pairing energy for each ligand type has the form $a_0 + a_4/r^4$.

The parameters are tuned to reproduce the calculated Fe-N bond lengths for both HS and LS complexes, plus the estimated HS-LS energy difference, ΔE_{HL}, derived from our earlier work (Supporting Information, Table S7). During this process, it became clear that the predicted Jahn-Teller distortion for **1** in its HS form depends on the nature of the metal-ligand π bonding and that this would facilitate choosing between the two suggested AOM parameter sets.

The HS $t_{2g}^4e_g^2$ configuration generates a complicated Jahn-Teller potential energy surface since the octahedral $^5T_{2g}$ ground state can couple both with e_g and t_{2g} vibrational modes leading to myriad possible minima.[47] Of course, $[Fe(bpp)_2]^{2+}$ is not octahedral. The highest symmetry is D_{2d} and for a d^6 system, the only possible *formally* Jahn-Teller active state is ^5E arising from the $e^2b_1^1b_2^1a_1^1$ d-electron configuration. The distinctive bonding characteristics of the bpp ligand means that ^5E is the lowest energy state in D_{2d} hence HS **1** is Jahn-Teller active. The relevant angles related to the Jahn-Teller distortions of **1** are shown in Figure 3.

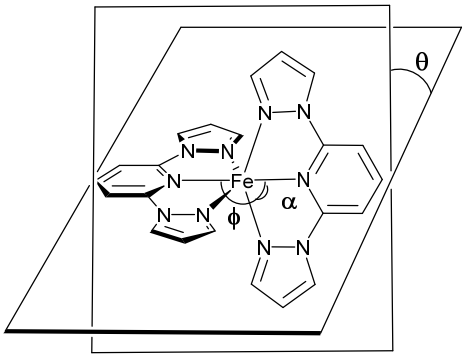

Figure 3 Definition of twisting angle, θ, tilting angle, ϕ, and bite angle, α, for $[Fe(bpp)_2]^{2+}$ (**1**).

For Set A (pyridine moderate π acceptor, pyrazole weak π donor), $\theta = 83.6$ °, $\phi = 169.9$ ° with $\alpha = 75.2$ ° for the bite associated with the shorter Fe-N(pyz) bond (2.17 Å) or 74.8 ° for the bite with the longer (2.20 Å) Fe-N(pyz). For Set B (both ligands moderate π donors), the angular structural parameters are $\theta = 88.8$ ° and $\phi = 179.9$ °. The two ligands are still inequivalent except now the difference is in the Fe-N(py) distances where one is distinctly shorter than the other (2.11 versus 2.15 Å). The one with the shorter bond has a slightly larger bite angle of 75.9 ° compared to 74.7 °.

As enumerated above, the ^5E degeneracy is raised by destroying the S_4 symmetry. Vertically displacing the bpp ligands relative to the metal as seen in the Set B distortion and shown schematically in the top right of Figure 4, generates an orbitally non-degenerate C_{2v} structure since the x and y axes are no longer equivalent. Likewise, varying θ from 90 ° and/or ϕ from 180 ° as in the Set A structure generates a C_2 geometry (Figure 4) which also achieves a lower, non-degenerate state.

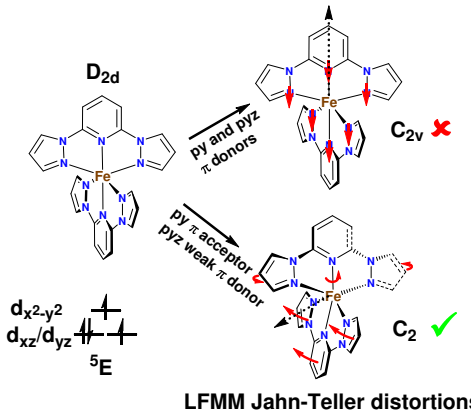

Figure 4 Schematic representation of the LFMM-computed Jahn-Teller distortions of HS $[Fe(bpp)_2]^{2+}$ as a function of the Fe-N π bonding. Red arrows represent the relative movements of the bpp ligands. The black dotted arrows show the C_2 axes.

The Set A distortion is typical of iron bis-pyrazolyl pyridine (bpp) complexes whereas the Set B distortion has never been reported. The LFMM method thus has the unique ability to use the computed structures to test various bonding scenarios and thus resolve ambiguous, fixed-geometry AOM parameter fitting when there is more than one way to achieve the same d orbital splitting pattern. These new results are more consistent with the pyridine donors in **1** acting as moderate π acceptor ligands contrary to the previous study[43b] based on the cellular ligand field (CLF) model where π-donor pyridines were assumed. The CLF approach was introduced by Deeth and Gerloch[48] to distinguish the 'ligand field' version of the AOM[42] from the Wolfsberg-Helmholtz MO version of Schäffer and Jorgensen.[21] However, for the present purposes, the CLF is essentially identical to the AOM and both treatments of metal-ligand π bonding are directly comparable. All subsequent LFMM results thus refer to the Set A parameters.

We expect the ^{5}E electronic state to couple to suitable vibrational modes to remove the orbital degeneracy. The three lowest energy vibrations in both DFT and LFMM comprise two equivalent motions which alter ϕ and one which alters θ (Figure 5) and these modes appear to be active here. In LS, the former are degenerate and there is a clean separation between ϕ and θ deformations. For HS, the symmetry is lower than D_{2d} but the modes are still cleanly separated for DFT while the rather more distorted LFMM HS structure mixes all three modes together. In particular, while the two modes at 38 cm^{-1} might be expected to be the two ν_ϕ modes, one of them is the only one of the three which shows any change in θ, hence the assignments shown in Table 3. The vibrational energies are comparable across both quantum and classical methods.

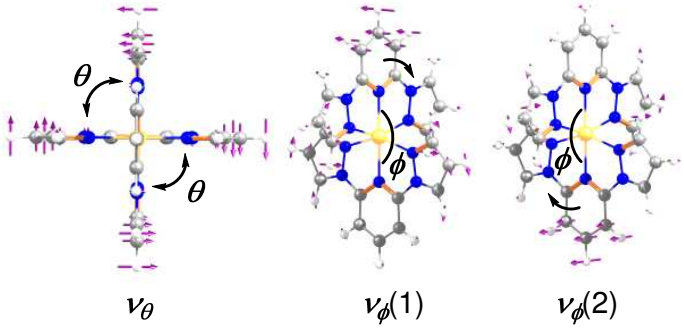

Figure 5 Three lowest calculated vibrational modes for $[Fe(bpp)_2]^{2+}$. Purple vectors represent relative atomic displacements.

Method/Spin	*DFT/HS*	*DFT/LS*	*LFMM/HS*	*LFMM/LS*
ν_θ	26	35	38	53
$\nu_\phi(1)$	13	40	21	49
$\nu_\phi(2)$	21	41	38	49

Table 3 Calculated vibrational mode energies for $[Fe(bpp)_2]^{2+}$. See Figure 5.

In passing, we note that related tridentate meridional-binding ligands such as, for example 2,2':6',2''-terpyridine or 2,6-di(pyrazol-3-yl)pyridine, present the same symmetry as bpp but may have different bonding properties which could lead to the Jahn-Teller inactive $^5B_1$ state. The combination of AILFT and LFMM probes the nature of the π bonding in such systems as well, and will be reported elsewhere.

SCO is well known to depend on crystal packing and LFMM can also be used to model the interactions between the $[Fe(bpp)_2]^{2+}$ complex and the counteranions. The Jahn-Teller instability of the ^5E parent state of **1** means that many apparently disparate structures may have similar energies. For example, the $[BF_4]^-$ salt of **1** appears to be much closer to D_{2d} symmetry with $\theta = 90$ ° and $\phi = 173$ ° compared to the $[PF_6]^-$ salt which is much more distorted with $\theta = 63$ ° and $\phi = 154$ °.

The LFMM-optimised structure for an isolated HS **1** complex has $\theta = 85$ ° and $\phi = 175$ ° which values are close to the experimental **1.**$[BF_4]_2$ values (see Figure 6 and Table 4). The local crystalline environment can be simulated by selected the four nearest $[A]^-$ counteranions to generate a $\{\mathbf{1}.[A]_4\}^{2-}$ cluster. With the anion coordinates frozen at their crystallographic positions, the LFMM-optimised HS structures for **1** change very little. That is, for $[A]^- = [BF_4]^-$, the more regular structure is retained while for $[A]^- = [PF_6]^-$, the distorted structure with θ far from 90 ° results. This is significant in that the LFMM does not force a geometry on the complex but rather responds (correctly) to its surroundings. Single point calculations with the counter-anions removed show that the distorted structure of **1** is 2.6 kcal/mol higher in energy. This value is also significant in two ways. Firstly, it is within the range of crystal packing energies. Secondly, the sign of the energy difference implies that the $[PF_6]^-$ system really is the distorted form and hence has a larger ΔE_{HL} than the $[BF_4]^-$ system. This is consistent with the former being observed to be HS in the range 5-300 K while the latter shows SCO behaviour with a $T_{1/2}$ of 261 K.[43b, 49]

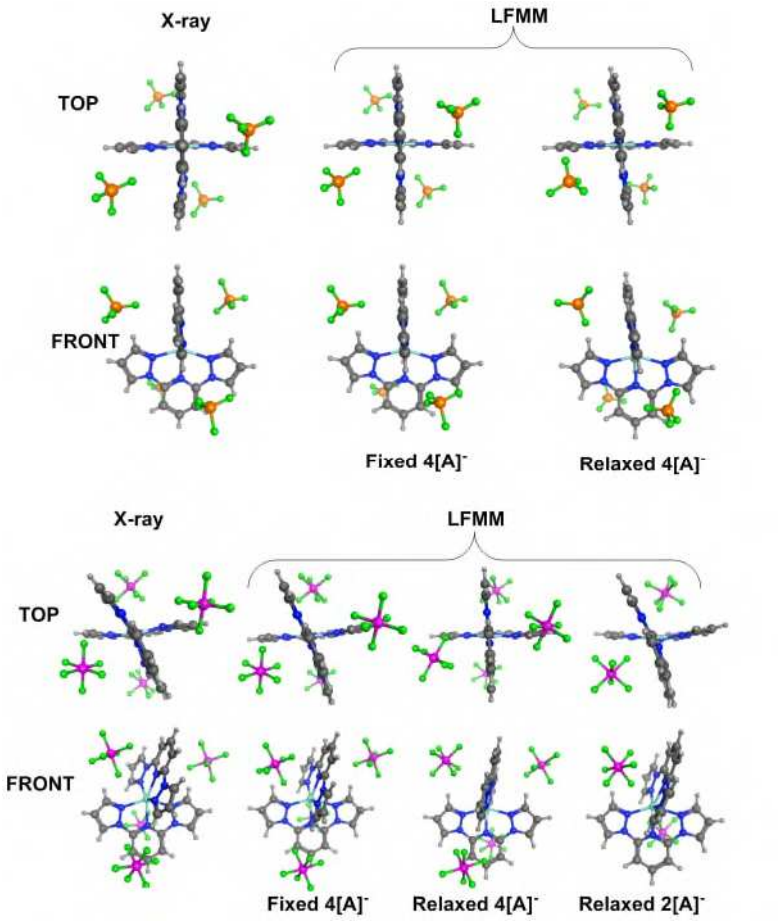

Figure 6 Effects of counteranions on LFMM optimised structure of **1**. Two views are shown, one from the top aligned along the Fe-N(pyridine) direction and one from the front at 90 ° to the top view. Counteranions ($[BF_4]^-$ or $[PF_6]^-$) are either held at their crystallographic positions (Fixed), or allowed to move (Relaxed). Values of θ and ϕ given in Table 4.

If the constraints on the anions are removed (labelled 'Relaxed 4[A]$^-$' in Figure 6), the structures of the metal complexes with either anion are almost the same. Both systems relax to the structure of the complex without any anions present and the distortion of the $[PF_6]^-$ system is lost. However, inspection of the experimental structure shows that two of the $[PF_6]^-$ anions are significantly closer to the cationic metal centre. If the LFMM calculation is repeated with just two anions, distorted structures closely related to the X-ray geometries with low θ values are predicted. A similar behaviour occurs with two $[BF_4]^-$ anions (Table 4). Overall, therefore, the LFMM FF appears to respond nicely to the local environment and provides a good description of the Jahn-Teller distortions for HS **1**. This bodes well for future development of LFMM with periodic boundary conditions and its applications to modelling SCO materials in the solid state.

Source	$[PF_6]^-$		$[BF_4]^-$	
	θ	ϕ	θ	ϕ
Exp.	63	154[a]	90	173
Fixed 4.[A]⁻	68	153	88	169
Relaxed 4.[A]⁻	85	166	85	167
Relaxed 2.[A]⁻	72	146	63	148
isolated	85	171	85	171

Table 4 Values for selected bond angles (see Figure 3) for $[Fe(bpp)_2]^{2+}$ in the presence or absence of counteranions, $[A]^-$ where A = PF_6 or BF_4.

We now explore how the LFMM FF performs on substituted bpp systems. Substituents at the pyrazole 3 positions should give rise to steric interactions between the R groups on one ligand and the pyridine moiety of the other. High spin complexes are expected and usually observed (Table 5).[50] For R = Me, the complex is HS in solution but in the solid state, both HS and SCO systems have been reported. Larger substituents give HS systems except in the case of R = mesityl which, perhaps unexpectedly given the HS behaviour for R = Ph, is LS.[51]

R	*Experimental*[51a]	ΔE_{HL}*(LFMM) (kcal/mol)*
Me	HS in solution Occasionally SCO in solid state	-2.8
CH_2OH	HS	-5.3
^iPr	HS	-7.5
Ph	HS	-8.7
CO_2Et	HS	-16.3
Mesityl	LS	+0.8

Table 5 Comparison of experimental behaviour (see ref [51a] and references therein) and LFMM spin state energy difference $\Delta E_{HL}(LFMM) = E_{HS}(LFMM) - E_{LS}(LFMM)$ (kcal/mol) for 3-substituted pyrazolyl $[Fe(bpp)_2]^{2+}$ complexes as a function of R group.

As shown in Table 5, the LFMM spin state energetics correlate very well with experimental observations. All R groups *except mesityl* are predicted, and observed, to generate HS systems. The additional dispersion interactions involving the mesityl methyl substituents are enhanced in the more compact LS structure leading to a theoretical prediction of LS behaviour overall. Moreover, of the HS systems, R = Me has the smallest $\Delta E_{HL}(LFMM)$ value which is within the nominal 3 kcal/mol crystal packing threshold, and is thus predicted to be the most likely to display SCO if the solid state packing is favourable. While the behaviour is quite complicated, examples of both HS and SCO salts of $[Fe(\mathbf{L}^1MeHH)_2]^{2+}$ have been reported.[52] The quality of the modelling is further evidenced by the overlays of the X-ray and LFMM structures for HS R=Ph and LS R = Mesityl shown in Figure 7.

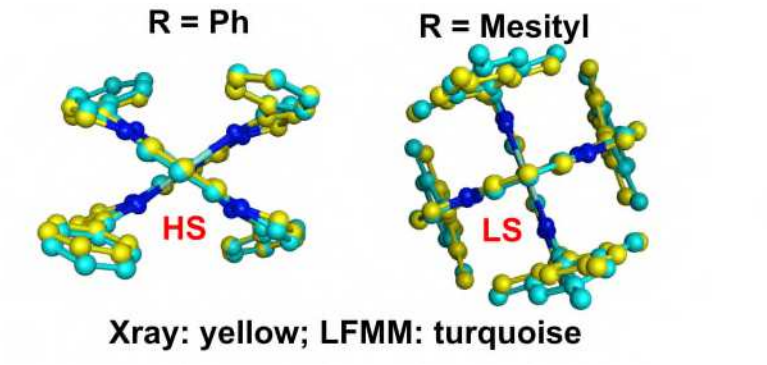

Figure 7 Overlays of LFMM-optimised and X-ray crystal structures for 3-substituted pyrazole complexes. Left: R = Ph, HS complex.[50b] Right: R = mesityl, LS complex.[51b] Hydrogens omitted.

Next, we consider the much more challenging cases of the 4-pyridyl and 4-pyrazolyl systems we had previously studied by DFT.[5b] The substituents are positioned to minimise any steric interactions and the magnetic moments are recorded in solution to remove solid-state packing effects. Variations of $T_{1/2}$ can thus be attributed to electronic effects exerted by the substituents which alter the metal-ligand bonding. Since the AOM parameters used for all complexes are the same, we do not expect the current LFMM FF to be able to model these effects correctly and, indeed, at first glance, there appears to be no correlation between the LFMM ΔE_{HL} values and the observed $T_{1/2}$ in solution (see Supporting Information Figure S1). However, if the analysis is separated into X substituents on the pyridines and the Y substituents on the pyrazoles, a modest correlation ($R^2 = 0.53$, see Supporting Information Figure S2) between the computed ΔE_{HL}(LFMM) values and the observed $T_{1/2}$ in solution is obtained, at least for X groups. However, this effect is electrostatic in origin (Supporting Information Figure S3) and is *opposite* to the desired behaviour in that the more electron withdrawing groups (EWGs) such as NO_2 present a positive dipole towards the cationic metal centre such that the shorter distances involved with LS systems lead to a relative destabilisation of the LS state (Figure 8). Thus, EWGs give the smallest ΔE_{HL}(LFMM) values (and hence would predict smaller $T_{1/2}$ values) as opposed to DFT and experiment where strong EWGs give larger ΔE_{HL} and hence a higher $T_{1/2}$.

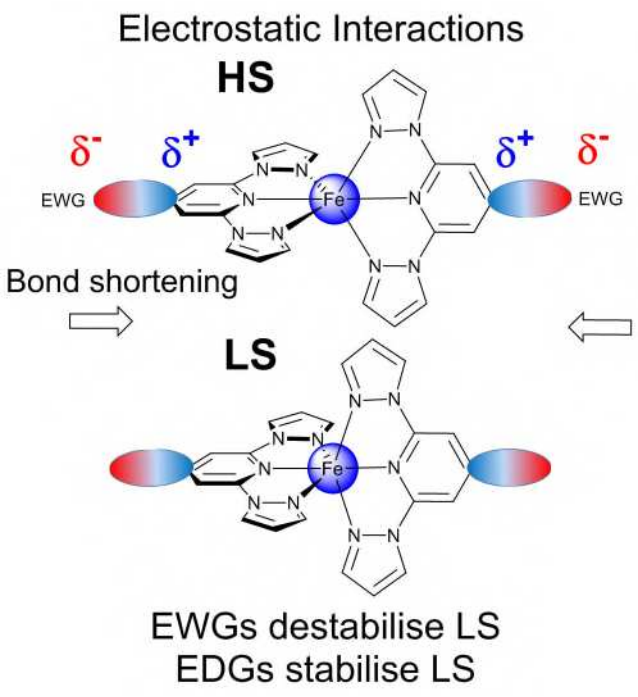

Figure 8 Electrostatic effect of charge polarisation arising from para substituents on the pyridine donor. Electron withdrawing groups present a positive dipole towards the cationic metal centre. The shorter dipole-metal distance in the LS complex leads to a more repulsive electrostatic interaction and a relative destabilisation of the LS state.

Substituents generate both an electrostatic and an electronic effect. For $[Fe(bpp)_2]^{2+}$ systems, the latter is dominant. DFT captures both effects and thus correlates well with experiment. The current LFMM FF only takes electrostatics into account which, in the case of X substituents on the π-accepting pyridine, has the opposite effect on ΔE_{HL} to that desired. Previous applications of LFMM to SCO systems focussed on amine donors connected by hydrocarbon backbones so this electrostatic effect was not significant.[15-16] For LFMM to deal correctly with SCO for more complicated conjugated ligand systems such as bpp, the electronic effect will need to be explicitly incorporated.

Conclusions

Force field parameter fitting is a perennial problem for classical molecular modelling methods. For LFMM, the extra burden can be reduced by using ab initio ligand field theory of Atanasov and Neese to generate theoretical d orbital energies ideally suited to fitting the AOM parameters of the LFMM.

Using $[Fe(bpp)_2]^{2+}$ as a model system, the AILFT predicts a splitting of the notional t_{2g} orbitals which can be reproduced in a number of Fe-N π bonding scenarios. However, the LFMM-optimised structure is only compatible with moderately π-accepting pyridines and relatively weak π-donor pyrazoles.

The sense of the computed Jahn-Teller distortion for HS $[Fe(bpp)_2]^{2+}$ is compatible with crystallographic observations and its magnitude depends on the interactions between the metal complex and the counter anions. The strong distortion observed for the $[PF_6]^-$ salt is seen to arise from the close approach of two anions. LFMM also captures the effects on the spin state energetics for 3-substituted pyrazoles, including the perhaps unexpected result that R = mesityl generates a LS system.

However, for 4-substituted pyridyl and pyrazolyl systems steric effects play virtually no role, and the solution $T_{1/2}$ values correlate with the substituent electronic effects. These are captured nicely by DFT but not by LFMM. Electronic effects thus have to be explicitly incorporated into LFMM if we are to model SCO for complexes of delocalised ligands correctly.

Acknowledgements

RJD acknowledges the generous support of Chemical Computing Group for the provision of MOE and Mihail Atanasov and Frank Neese for pre-release access to the AILFT code in ORCA. The authors acknowledge the funding of the EPSRC for the Critical Mass grant *Understanding and engineering function in switchable molecular crystals* (EP/K012940; EP/K012568, EP/K012576, EP/K013009) as well as the many stimulating interactions with members of the COST Action CM1305 *Explicit control over spin states in Technology and Biochemistry* (ECOSTBio).

References

[1] a) M. A. Halcrow in *Spin-Crossover Materials: Properties and Applications*, *Vol.* Wiley-Blackwell, Chichester, UK, **2013**, p. 564; b) P. Gutlich, Y. Garcia and H. A. Goodwin, *Chem. Soc. Rev.* **2000**, *29*, 419-427; c) P. Gutlich, A. Hauser and H. Spiering, *Angew. Chem. Int. Ed.* **1994**, *33*, 2024-2054.
[2] a) O. Kahn and C. J. Martinez, *Science* **1998**, *279*, 44-48; b) A. Bousseksou, G. Molnar and G. Matouzenko, *Eur. J. Inorg. Chem.* **2004**, 4353-4369; c) I. Suleimanov, G. Molnár, L. Salmon and A. Bousseksou, *Eur. J. Inorg. Chem.* **2017**, *2017*, 3446-3451; d) M. D. Manrique-Juarez, F. Mathieu, V. Shalabaeva, J. Cacheux, S. Rat, L. Nicu, T. Leïchlé, L. Salmon, G. Molnár and A. Bousseksou, *Angew. Chem. Int. Ed.* **2017**, *56*, 8074-8078; e) C. Lefter, S. Rat, J. S. Costa, M. D. Manrique-Juarez, C. M. Quintero, L. Salmon, I. Seguy, T. Leichle, L. Nicu, P. Demont, A. Rotaru, G. Molnar and A. Bousseksou, *Adv. Mater.* **2016**, *28*, 7508-7514.
[3] Y. Garcia and P. Gütlich in *Thermal Spin Crossover in Mn(II), Mn(III), Cr(II) and Co(III) Coordination Compounds*, *Vol. 234* Springer Berlin Heidelberg, **2004**, pp. 49-62.

[4] a) L. Cambi and A. Cagnasso, *Atti Accad. Naz. Lincei* **1931**, *13*, 809; b) W. A. Baker and H. M. Bobonich, *Inorg. Chem.* **1964**, *3*, 1184.
[5] a) P. Gütlich, *Eur. J. Inorg. Chem.* **2013**, *2013*, 581-591; b) L. J. Kershaw Cook, R. Kulmaczewski, R. Mohammed, S. Dudley, S. A. Barrett, M. A. Little, R. J. Deeth and M. A. Halcrow, *Angew. Chem.* **2016**, *128*, 4399-4403; c) M. A. Halcrow, *Crystals* **2016**, *6*; d) J. Elhaïk, C. A. Kilner and M. A. Halcrow, *Eur. J. Inorg. Chem.* **2014**, *2014*, 4250-4253; e) J. A. Kitchen and S. Brooker, *Coord. Chem. Rev.* **2008**, *252*, 2072-2092.
[6] J. H. Van Vleck, *J. Chem. Phys.* **1935**, *3*, 807.
[7] B. Li, R.-J. Wei, J. Tao, R.-B. Huang and L.-S. Zheng, *Inorg. Chem.* **2009**, *49*, 745-751.
[8] S. Decurtins, P. Gütlich, C. P. Köhler, H. Spiering and A. Hauser, *Chem. Phys. Lett.* **1984**, *105*, 1-4.
[9] M. A. Halcrow, *Polyhedron* **2007**, *26*, 3523-3576.
[10] a) R. J. Deeth in *Molecular Discovery in Spin Crossover*, John Wiley & Sons, Ltd, Chichester, UK **2016**, 85-102; b) L. M. L. Daku, F. Aquilante, T. W. Robinson and A. Hauser, *J. Chem. Theory. Comput.* **2012**, *8*, 4216-4231; c) S. F. Ye and F. Neese, *Inorg. Chem.* **2010**, *49*, 772-774; d) K. Pierloot, Q. M. Phung and A. Domingo, *J. Chem. Theory. Comput.* **2017**, *13*, 537-553; e) K. P. Kepp, *Inorg. Chem.* **2016**, *55*, 2717-2727; f) K. P. Kepp, *Coord. Chem. Rev.* **2013**, *257*, 196-209.
[11] B. J. Houghton and R. J. Deeth, *Eur. J. Inorg. Chem.* **2014**, *2014*, 4573-4580.
[12] R. K. Hocking, R. J. Deeth and T. W. Hambley, *Inorg. Chem.* **2007**, *46*, 8238 -8244.
[13] a) H. Paulsen, V. Schuenemann and J. A. Wolny, *Eur. J. Inorg. Chem.* **2013**, 628-641; b) H. Paulsen and A. X. Trautwein, *J. Phys. Chem. Solids* **2004**, *65*, 793-798.
[14] a) V. J. Burton, R. J. Deeth, C. M. Kemp and P. J. Gilbert, *J. Am. Chem. Soc.* **1995**, *117*, 8407-8415; b) R. J. Deeth, *Coord. Chem. Rev.* **2001**, *212*, 11-34.
[15] a) C. M. Handley and R. J. Deeth, *J. Chem. Theory. Comput.* **2012**, *8*, 194-202; b) R. J. Deeth, A. E. Anastasi and M. J. Wilcockson, *J. Am. Chem. Soc.* **2010**, *132*, 6876–6877.
[16] M. Foscato, B. J. Houghton, G. Occhipinti, R. J. Deeth and V. R. Jensen, *J. Chem. Inf. Mod.* **2015**, *55*, 1844-1856.
[17] Bernhardt, P.; Deeth, R. J.; Jensen, V. R.; Thörnroos, K. W., Riley, M.; Foscato, M., in preparation
[18] a) P. Comba and R. Remenyi, *Coord. Chem. Rev.* **2003**, *238*, 9-20; b) P. O. Norrby and P. Brandt, *Coord. Chem. Rev.* **2001**, *212*, 79-109.
[19] A. K. Rappe, C. J. Casewit, K. S. Colwell, W. A. Goddard and W. M. Skiff, *J. Am. Chem. Soc.* **1992**, *114*, 10024-10035.
[20] R. J. Deeth, A. Anastasi, C. Diedrich and K. Randell, *Coord. Chem. Rev.* **2009**, *253*, 795-816.
[21] C. E. Schaeffer and C. K. Jorgensen, *Mol. Phys.* **1965**, *9*, 401.
[22] a) K. A. H. Alzahrani and R. J. Deeth, *J. Mol. Model.* **2016**, *22*, 1-13; b) R. Brodbeck and R. J. Deeth, *Dalton Trans.* **2011**, *40*, 11147-11155; c) R. J. Deeth, R. VanEldik and J. Harvey, *Advances in Inorganic Chemistry: Theoretical and Computational Inorganic Chemistry, Vol 62* **2010**, *62*, 1-39.
[23] R. J. Deeth and D. L. Foulis, *PCCP* **2002**, *4*, 4292-4297.
[24] a) S. K. Singh, J. Eng, M. Atanasov and F. Neese, *Coord. Chem. Rev.* **2017**, *344*, 2-25; b) M. Atanasov, J. M. Zadrozny, J. R. Long and F. Neese, *Chemical Science* **2013**, *4*, 139-156; c) M. Atanasov, D. Ganyushin, K. Sivalingam and F. Neese in *A Modern First-Principles View on Ligand Field Theory Through the Eyes of Correlated Multireference Wavefunctions*, *Vol. 143* Eds.: D. M. P. Mingos, P. Day and J. P. Dahl), **2012**, pp. 149-220.
[25] F. Neese, U. Becker, D. Ganiouchine, S. Koßmann, T. Petrenko, C. Riplinger and F. Wennmohs in *ORCA: program version 3.0*, *Vol.* Max Planck Institute for Chemnical Energy Conversion, Muellheim, **2014**.

[26] a) J. Jung, M. Atanasov and F. Neese, *Inorg. Chem.* **2017**, *56*, 8802-8816; b) M. Atanasov, D. Ganyushin, K. Sivalingam and F. Neese in *A Modern First-Principles View on Ligand Field Theory Through the Eyes of Correlated Multireference Wavefunctions*, Eds.: D. M. P. Mingos, P. Day and J. P. Dahl), Springer Berlin Heidelberg, Berlin, Heidelberg, **2012**, pp. 149-220.
[27] a) A. D. Becke, *Phys. Rev. A* **1988**, *38*, 3098-3100; b) J. P. Perdew and W. Yue, *Phys. Rev. B-Condensed Matter* **1986**, *33*, 8800-8802.
[28] A. Schaefer, H. Horn and R. Ahlrichs, *J. Chem. Phys.* **1992**, *97*, 2571.
[29] A. Klamt and G. Schüürmann, *J. Chem. Soc., Perkin Trans.* **1993**, *2*, 799.
[30] C. Daul, *J. Comput. Chem.* **1994**, *52*, 867.
[31] T. Ziegler, A. Rauk and E. J. Baerends, *Theoret. Chim. Acta* **1977**, *43*, 261.
[32] J. C. Slater, *The Self-consistent Field for Molecules and Solids*, McGraw-Hill, USA, **1974**, p.
[33] a) A. Atanasov, C. A. Daul and C. Rauzy in *A DFT based ligand field theory*, *Vol. 106* Springer Verlag, Berlin, **2004**, pp. 97-125; b) M. Atanasov, C. A. Daul and C. Rauzy, *Chem. Phys. Lett.* **2003**, *367*, 737-746; c) M. Atanasov and C. A. Daul, *Chem. Phys. Lett.* **2003**, *379*, 209-215; d) M. Atanasov and C. A. Daul, *Chem. Phys. Lett.* **2003**, *381*, 584-591.
[34] a) F. Vlahović, M. Perić, M. Gruden-Pavlović and M. Zlatar, *J. Chem. Phys.* **2015**, *142*, 214111; b) M. Gruden-Pavlovic, M. Peric, P. Garcia Fernandez and M. Zlatar, *Chemical Science* **2013**.
[35] R. G. Woolley, *Mol. Phys.* **1981**, *42*, 703-720.
[36] a) R. J. Deeth and M. Gerloch, *Inorg. Chem.* **1985**, *24*, 1754-1758; b) R. J. Deeth and M. Gerloch, *Inorg. Chem.* **1984**, *23*, 3846-3853; c) R. J. Deeth and M. Gerloch, *Inorg. Chem.* **1984**, *23*, 3853-3861.
[37] D. A. Cruse, J. E. Davies, M. Gerloch, J. H. Harding, D. J. Mackey and R. F. McMeeking in *CAMMAG*, *Vol.* Cambridge, **1983**.
[38] V. G. Chilkuri, S. DeBeer and F. Neese, *Inorg. Chem.* **2017**, *56*, 10418-10436.
[39] R. J. Deeth, N. Fey and B. J. Williams-Hubbard, *J. Comput. Chem.* **2005**, *26*, 123-130.
[40] MOE in *Molecular Operating Environment*, *Vol.* Chemical Computing Group, Montreal, **2015**.
[41] B. N. Figgis and M. A. Hitchman, *Ligand Field Theory and Its Applications*, John Wiley and Sons Ltd., New York, **2000**, p.
[42] M. Gerloch and R. G. Woolley, *Prog. Inorg. Chem.* **1983**, *31*, 371-446.
[43] a) C. Carbonera, C. A. Kilner, J. F. Letard and M. A. Halcrow, *Dalton Trans.* **2007**, 1284-1292; b) J. M. Holland, J. A. McAllister, C. A. Kilner, M. Thornton-Pett, A. J. Bridgeman and M. A. Halcrow, *J. Chem. Soc., Dalton Trans.* **2002**, 548-554.
[44] M. J. Riley, *Inorg. Chim. Acta* **1998**, *268*, 55-62.
[45] E. A. Suturina, D. Maganas, E. Bill, M. Atanasov and F. Neese, *Inorg. Chem.* **2015**, *54*, 9948-9961.
[46] a) T. A. Halgren and R. B. Nachbar, *J. Comput. Chem.* **1996**, *17*, 587-615; b) T. A. Halgren, *J. Comput. Chem.* **1996**, *17*, 553-586; c) T. A. Halgren, *J. Comput. Chem.* **1996**, *17*, 520-552; d) T. A. Halgren, *J. Comput. Chem.* **1996**, *17*, 490-519.
[47] R. J. Deeth, A. Anastasi and K. Randell, *Dalton Trans.* **2009**, 6007-6012.
[48] R. J. Deeth and M. Gerloch, *J. Chem. Soc., Dalton Trans.* **1986**, 1531-1534.
[49] S. Vela, M. Fumanal, J. Ribas-Arino and V. Robert, *PCCP* **2015**, *17*, 16306-16314.
[50] a) J. M. Holland, S. A. Barrett, C. A. Kilner and M. A. Halcrow, *Inorg. Chem. Commun.* **2002**, *5*, 328-332; b) J. Elhaik, D. J. Evans, C. A. Kilner and M. A. Halcrow, *Dalton Trans.* **2005**, 1693-1700.

[51] a) M. A. Halcrow, *Coord. Chem. Rev.* **2009**, *253*, 2493-2514; b) F. Pelascini, M. Wesolek, F. Peruch, A. D. Cian, N. Kyritsakas, P. J. Lutz and J. Kress, *Polyhedron* **2004**, *23*, 3193-3199.
[52] V. A. Money, C. Carbonera, J. Elhaik, M. A. Halcrow, J. A. K. Howard and J. F. Letard, *Chem. Eur. J.* **2007**, *13*, 5503-5514.